AIP | Applied Physics Letters

Defect-enhanced photoconductive response of silicon-implanted borosilicate glass

Gong-Ru Lin, Chun-Jung Lin, and Chi-Kuan Lin

Citation: Applied Physics Letters **85**, 935 (2004); doi: 10.1063/1.1779945
View online: http://dx.doi.org/10.1063/1.1779945
View Table of Contents: http://scitation.aip.org/content/aip/journal/apl/85/6?ver=pdfcov
Published by the AIP Publishing

Articles you may be interested in

Defect reduction in silicon nanoparticles by low-temperature vacuum annealing
Appl. Phys. Lett. **96**, 193112 (2010); 10.1063/1.3428359

Publisher's Note: "Defect-enhanced photoconductive response of silicon-implanted borosilicate glass" [Appl. Phys. Lett.85, 935 (2004)]
Appl. Phys. Lett. **85**, 3325 (2004); 10.1063/1.1804499

Effect of low-temperature annealing on the luminescent lifetime and negative differential resistance of silicon-implanted borosilicate glass
J. Appl. Phys. **94**, 7542 (2003); 10.1063/1.1630366

Evolution of photoluminescent defect clusters in proton- and copper-implanted silicon crystals during annealing
J. Appl. Phys. **94**, 3075 (2003); 10.1063/1.1593801

Differences in the densities of charged defect states and kinetics of Staebler–Wronski effect in undoped (nonintrinsic) hydrogenated amorphous silicon thin films
J. Appl. Phys. **81**, 3526 (1997); 10.1063/1.365000

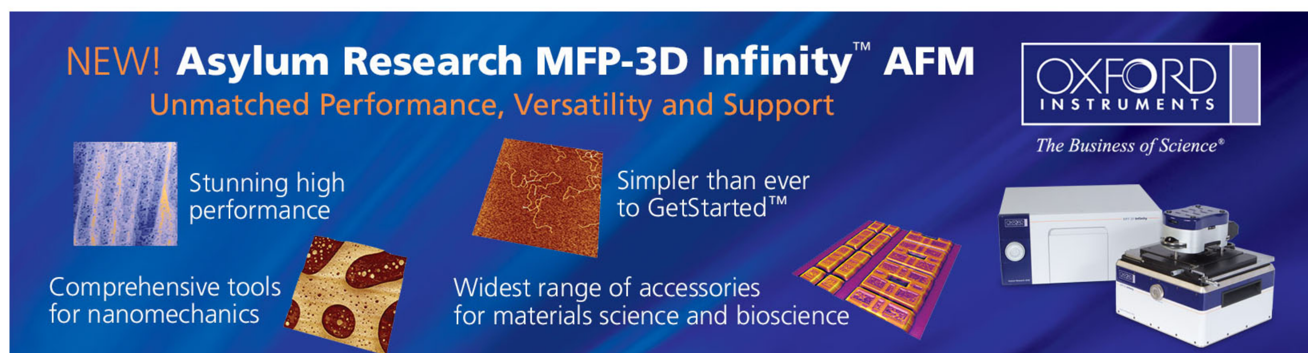

This article is copyrighted as indicated in the article. Reuse of AIP content is subject to the terms at: http://scitation.aip.org/termsconditions. Downloaded to IP: 140.113.38.11 On: Thu, 01 May 2014 04:15:37

HTML ABSTRACT + LINKS

Defect-enhanced photoconductive response of silicon-implanted borosilicate glass

Gong-Ru Lin,[a] Chun-Jung Lin, and Chi-Kuan Lin
Institute of Electro-Optical Engineering, National Chiao Tung University, 1001, Ta Hsueh Road, Hsinchu, Taiwan 300, Republic of China

(Received 29 December 2003; accepted 16 June 2004; publisher error corrected 21 August 2004)

The E'_{δ}-defect-enhanced photoconductivity of a metal–semiconductor–metal photodetector (MSM-PD) made on Si-implanted borosilicate glass ($BSO:Si^+$) substrate is reported. The dark current of as-implanted $BSO:Si^+$ MSM-PD is only 0.1 nA at bias of 70 V. The photocurrent of as-implanted $BSO:Si^+$ MSM-PD illuminated at 488 nm is 0.91 nA, corresponding to photoconductive gain of 9.1 dB. The E'_{δ}-defects luminescent at 520 nm are activated after 2 h annealing, which enhances the photocurrent of $BSO:Si^+$ MSM-PD by one order of magnitude. Optimized responsivity, noise equivalent power, and detectivity of $BSO:Si^+$ MSM-PD are $4.0\ \mu A/W$, $1.2\times10^{-9}\ W/Hz^{1/2}$, and $3.5\times10^{5}\ cm\,Hz^{1/2}/W$, respectively. The electron paramagnetic resonance and etching-dependent photocurrent analysis corroborate the E'_{δ}-defect-related photoconductivity of the $BSO:Si^+$ glass. *© 2004 American Institute of Physics*. [DOI: 10.1063/1.1779945]

Si-rich SiO_2 materials were synthesized for potential applications in white-light emitting devices.[1,2] The Si implantation is the most intriguing technique[3] since which provides a precise control for the density and distribution of the excess Si ion in SiO_2. Thermal annealing facilitates the activation of irradiative defects in Si-implanted SiO_2 ($SiO_2:Si^+$), such as the E'_{δ} defect (a precursor of nanocrystallite Si)[4] with photoluminescence (PL) at 520–550 nm, and the nonbridge oxygen hole center[5] with PL at 610–650 nm. High-temperature (usually $>1000\ °C$) and long-term annealing further leads to the quenching of defect-related PL and to the formation of nanocrystallite Si (nc-Si) in $SiO_2:Si^+$. The studies on the photocurrent response of $SiO_2:Si^+$ and Si-implanted borosilicate glass ($BSO:Si^+$)[6,7] were previously investigated. Choi *et al.*[8] observed a negative photoconductivity in a metal–$SiO_2:Si^+$–Si diode with dense nc-Si under UV illumination. Hirano *et al.*[9] studied the photoconductivity of the Si/SiO_2 multilayers containing nc-Si with a size of 3–5 nm. Coffa *et al.*[10] demonstrated the charge storage and negative photoconductivity of nc-Si embedded in SiO_2/p-Si. These results suggest a strong correlation between the nc-Si and the anomalous photoconductivity. Nevertheless, there were few reports on the defect-related photoconductivity of these materials. In this work, the wavelength-dependent blue–green photoconductivity of an interdigitized metal–$BSO:Si^+$-metal photodetector (MSM-PD) is characterized. A strong correlation between the E'_{δ}-defect-enhanced photocurrent and the depth distribution profile of excess Si atoms in $BSO:Si^+$ is elucidated.

The $BSO:Si^+$ samples were prepared by multienergy Si implanting the 125-μm-thick BSO glass at 50, 100, and 200 keV with a constant dosage of $10^{16}\ ions/cm^2$. The $BSO:Si^+$ samples were encapsulated annealing in quartz furnace with forming gas at 500 °C from 1 to *4* h at 1 h increment. Afterward, the $BSO:Si^+$ MSM-PDs with 150-nm-thick aluminum Schottky contacts and five interdigitized finger electrodes were fabricated. The finger width (and spacing), and the active area of the MSM-PD are 5 μm and $50\times50\ \mu m^2$, respectively (see Fig. 1). The photocurrent was measured using a programmable electrometer (Keithley, model 6517) with resolution as low as 100 fA. The capacitance of the $BSO:Si^+$ MSM-PD is about 0.1 pF at bias of 45 V. The MSM-PD was illuminated by a white-light laser with output power and focused spot size of 1.5 mW and 50 μm, respectively. The responsivity R of the MSM-PD is calculated using

$$R=\frac{(I_{\mathrm{photo}}-I_{\mathrm{dark}})}{P_{\mathrm{laser}}\cdot(A_{\mathrm{MSM-PD}}/A_{\mathrm{laser}})}, \tag{1}$$

where I^{photo} and I_{dark} denote the photo- and dark- current of the $BSO:Si^+$ MSM-PD, A_{laser} is the area of the focused laser spot, $A_{\mathrm{MSM\text{-}PD}}$ is the active area of the MSM-PD, and P_{laser} is the laser power at the illuminating end. The noise equivalent power [(NEP) defined as the ratio of output noise to responsivity] of $BSO:Si^+$ MSM-PD is defined as $\mathrm{NEP}=(I_n/R)=(1/R)(2eI_dB)^{0.5}$, where I_n is the detected current, e is the electron charge, I_d is the dark current, and B is the operational bandwidth of $B=(1/2\pi)(r\times C)$ with r and C denoting

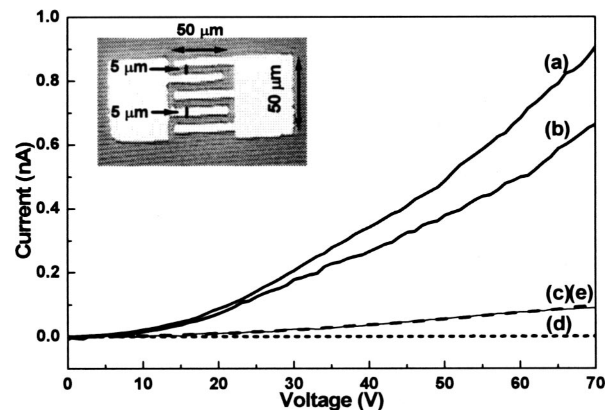

FIG. 1. Photocurrent of as-implanted $BSO:Si^+$ MSM-PD at wavelength of: (a) 488 nm and (b) 514.5 nm under 1.5 mW illumination as compared to the dark current of MSM-PD on (c) as-implanted $BSO:Si^+$, (d) unprocessed BSO glass, and (e) illuminated as-implanted $BSO:Si^+$. The inset is the pattern of $BSO:Si^+$ MSM-PD.

[a]Electronic mail: grlin@faculty.nctu.edu.tw

This article is copyrighted as indicated in the article. Reuse of AIP content is subject to the terms at: http://scitation.aip.org/termsconditions. Downloaded to IP: 140.113.38.11 On: Thu, 01 May 2014 04:15:37

 © 2004 American Institute of Physics

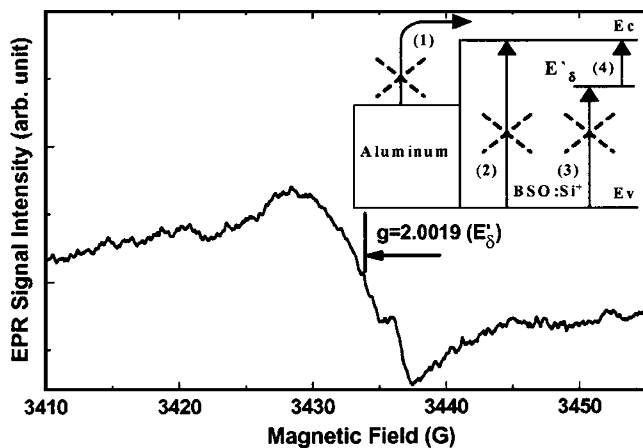

FIG. 2. EPR spectrum of the 2 h annealed BSO:Si$^+$. The inset illustrates the possible photoelectron transport of BSO:Si$^+$ MSM-PD. (1) The thermionic emission of Aluminum-BSO:Si$^+$ junction. (2) The band-to-band transition of BSO:Si$^+$. (3) The hole emission from E'_δ-defect level. (4) The electron emission from the E'_δ-defect level.

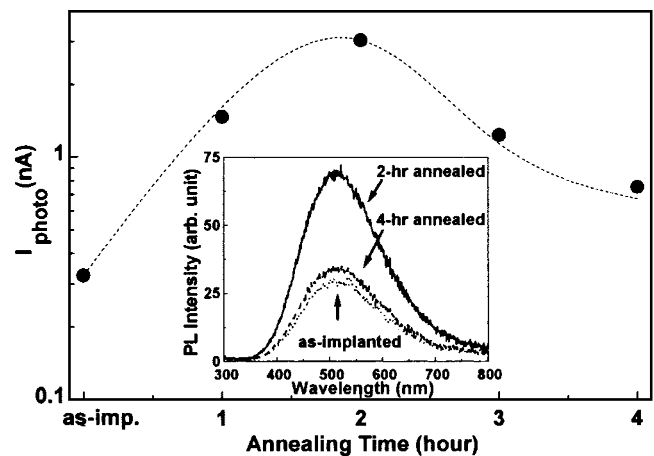

FIG. 4. Photocurrent of MSM-PD with 5 μm gap spacing on as-implanted BSO:Si$^+$ as a function of annealing time at $V_{\text{bias}}=45$ V under illumining wavelength and power of 514.5 nm and 1.5 mW. The inset is the PL spectra of BSO:Si$^+$ annealed at 500 °C for different annealing times.

the resistance and capacitance of MSM-PD, respectively. The detectivity D^* is defined as $D^*=(AB)^{0.5}/\text{NEP}$. A buffered oxide etching (BOE) solution ($NH_4F:HF=6:1$ with an etching rate of 100 nm/s) for the BSO:Si$^+$ is used to study the depth-dependent photoconductivity.

The dark current of as-implanted BSO:Si$^+$ at bias of 70 V is 0.1 nA, which is ten times larger than the BSO glass (see Fig. 1). The enlarged dark current results from hopping conduction among defects or surface enhanced tunneling (due to the reduction in junction barrier height). The wavelength-dependent photocurrent response of the as-implanted BSO:Si$^+$ MSM-PD is also observed. The absorption coefficient of the BSO:Si$^+$ is $\leqslant 10^{-3}$ cm^{-1} in visible wavelength, avoiding the illumination-induced substrate heating effect. This is confirmed by the unchanged dark current response of the as-implanted BSO:Si$^+$ before and after illumination. The photocurrent of as-implanted BSO:Si$^+$ MSM-PD is 0.66 nA at 514.5 nm, corresponding to the photocurrent gain ($I_{\text{photo}}/I_{\text{dark}}$) and optical responsivity of 6.6 dB and 0.74 μA/W, respectively. Illuminating at a shorter wavelength further improves the photocurrent response. As shown in Fig. 2, the thermionic emission at the aluminum–BSO junction barrier requires energy of 3.38 eV, the bandgap energy of BSO is 8.9 eV, and the hole emission from the E'_δ-defect level requires an energy of 6.49 eV. Obviously, the pumping energy of 2.54 eV is only sufficient to excite electrons from the E'_δ defect[11] to the conduction band of BSO:Si$^+$. The electron paramagnetic resonance (EPR) analysis corroborates the complete activation of E'_δ defects in 2 h annealed BSO:Si$^+$ (see Fig. 2),[12–14] which reveals a zero-crossing g value of 2.0019. The generation of E'_δ defects after implantation and annealing is confirmed by PL analysis. (see Fig. 3) Since the energy distribution of the E'_δ-defect level in BSO:Si$^+$ is relatively broadened, the photoconductivity becomes observable when the pumping wavelength is shorter than 587 nm. A higher-energy excitation of the BSO:Si$^+$ MSM-PD alternatively provides the carriers with large kinetic energy to tunnel through defects. To verify these two possibilities, the wavelength-dependent photocurrent response of the BSO:Si$^+$ MSM-PD at bias of 50 V is performed, as shown in Fig. 4. The optical responsivity of the BSO:Si$^+$ MSM-PD increases as the illuminating wavelength shortens, which saturates at near-UV region with a maximum value of 0.5 nA (corresponding to 0.55 μA/W). The photocurrent diminishes at a wavelength beyond 650 nm. The equivalent defect density obtained from the integral of PL spectra coincides well with the wavelength-dependent profile of photocurrent response.

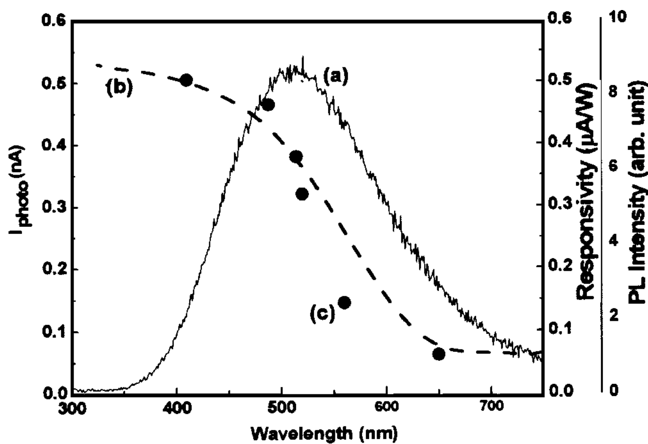

FIG. 3. (a) The PL spectrum of as-implanted BSO:Si$^+$ MSM-PD, (b) the equivalent defect density obtained from the integral of PL spectrum, and (c) the wavelength dependence of the photocurrent and responsivity for the as-implanted BSO:Si$^+$ MSM-PD.

As the annealing time is prolonged to 2 h, the maximum PL intensity contributed by the activated E'_δ defects at 520 nm in BSO:Si$^+$ is obtained (see the inset of Fig. 4). However, the elimination of these defects at longer annealing durations inevitably leads to a decreasing photocurrent response. After 4 h of annealing, the photocurrent of BSO:Si$^+$ MSM-PD illuminated at 514.5 nm significantly decreases from 3.1 nA (maximum value at 2 h annealing condition) to 0.7 nA. The EPR analysis also reveals the long-term annealing-induced reduction in E'_δ-defect density due to oxidation effect. These observations correlate well with the degrading photoconductivity of the 4 h annealed BSO:Si$^+$ sample. This correlates well with the decreasing trend of the PL results, which again corroborates the quenching of the defects during long-term annealing process. In addition, the redshift of peak PL wavelength is not found in annealed BSO:Si$^+$, which means that the excess Si ions or the E'_δ

This article is copyrighted as indicated in the article. Reuse of AIP content is subject to the terms at: http://scitation.aip.org/termsconditions. Downloaded to IP: 140.113.38.11 On: Thu, 01 May 2014 04:15:37

TABLE I. The figures of merits of BSO:Si$^+$ MSM-PD biased at 45 V and illuminated at 514.5 nm. R: responsivity, NEP: noise equivalent power, D^*: detectivity.

Condition	R (μA/W)	NEP (W/Hz$^{1/2}$)	D^* (cm Hz$^{1/2}$/W)
As-implanted	0.37	1.1×10^{-8}	3.6×10^{4}
2 h annealed	4.0	1.2×10^{-9}	3.5×10^{5}

defects (the precursors of the nanocrystallite Si) are finally oxidized instead of forming nc-Si under such a low annealing temperature. By taking the measured responsivity $R=0.37\ \mu$A/W, the NEP, and D^* of the as-implanted BSO:Si$^+$ MSM-PD are 1.1×10^{-8} (W/Hz$^{1/2}$) and 3.6×10^{4} (cm Hz$^{1/2}$/W), which become 1.2×10^{-9} (W/Hz$^{1/2}$) and 3.5×10^{5} (cm Hz$^{1/2}$/W) as R increases to 4.0 A/W after 2 h of annealing, as listed in Table I. To further realize the effect of distributed defects on the photocurrent response of the BSO:Si$^+$ MSM-PD, the BSO:Si$^+$ substrates were etched by a BOE solution with the etching depth changing from 100 to 300 nm at a 100 nm incensement prior to the fabrication of MSM-PD, and then MSM patterns are fabricated on the BSO:Si$^+$ samples. The photocurrent of the MSM-PD made on 100-nm-etched BSO:Si$^+$ becomes at least twice larger than that made on original BSO:Si$^+$ (see Fig. 5), which is mainly attributed to the removal of surface oxide layer after etching. The distribution profile of excess Si atoms is a Gaussian-type function and the implanted density of Si atoms is extremely small beneath the BSO glass surface with a layer thickness of about 10 nm according to the *TRIM* simulation. A tunneling-like carrier transport is required through such a thin layer with same insulating property as the original BSO glass. The etching process releases the tunneling transport of a photoexcited carrier from BSO:Si$^+$ to the surface contact by removing the thin insulating layer. Nonetheless, the photocurrent eventually decreases when the BSO:Si$^+$ surface is overetched, which strongly correlates well with the depth profile of the implanting dose.

Previously, Choi and Elliman[8] reported a different negative photoconductivity phenomenon in the metal–insulator–semiconductor (MIS) diode made on SiO_2:Si$^+$/p-Si containing nc-Si, where the photoionized electrons from the oxide/nc-Si layer recombine with holes in the accumulation layer formed at the SiO_2:Si$^+$/Si interface under forward bias. The nc-Si in the SiO_2:Si$^+$ is then positively charged by the remaining hole, which eventually screens the bias voltage and results in a decreasing photocurrent at a certain voltage. If the current decreased by this effect becomes larger than the current increased by the photoexcitation of extra holes in the accumulation layer, the negative photoconductivity is observed. Coffa *et al.*[10] also confirmed that the observed negative photoconductivity (if larger than the current caused by the photoexcitation of carriers) is mainly contributed by the nc-Si embedded in the SiO_2:Si$^+$ layer after a subsequent annealing at 1000 °C for 1 h in flowing argon gas. However, in our experiment, the phenomenon of negative photoconductivity is not found, since the annealing temperature of our BSO:Si$^+$ sample is much lower than that in Choi's experiment. In contrast, the BSO:Si$^+$ MSM-PD behaves rather like a double-barrier (MIS–insulator–metal) tunneling diode made on defect-rich substrate. The carrier transport mechanism is completely different from that of the MIS diode made on the SiO_2:Si$^+$/Si with nc-Si. The photocurrent of BSO:Si$^+$ MSM-PD increases with the higher bias voltage and shorter wavelength. This again proves that there are no Si nanocrystals in the BSO:Si$^+$ MSM-PD and the enhanced photocurrent is not caused by the nc-Si in the BSO:Si$^+$.

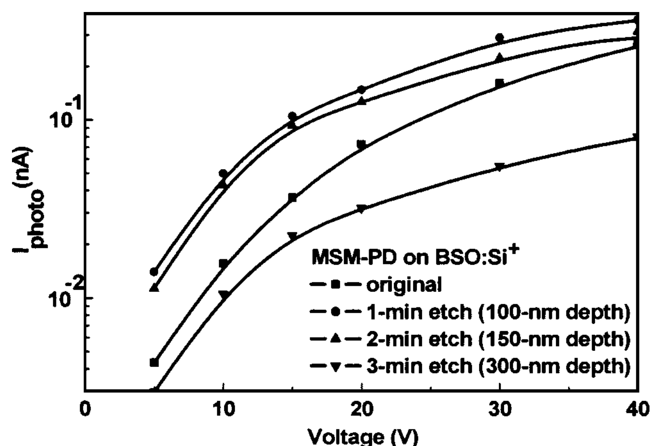

FIG. 5. Photocurrent–voltage response of the MSM-PD made on buried oxide-etched BSO:Si$^+$ substrate.

In conclusion, the defect-enhanced photoconductive response in BSO:Si$^+$ was reported. The low-temperature annealing excludes the formation of nc-Si in BSO:Si$^+$. The dominant defects (E'_δ defects) corresponding to the wavelength at 520 nm are activated during 2 h of annealing, which leads to an optimization of photocurrent of a BSO:Si$^+$ MSM-PD. The optimized responsivity R, NEP, and D^* of 2 h annealed BSO:Si$^+$ MSM-PD at bias of 45 V are 4.0 μA/W, 1.2×10^{-9} W/Hz$^{1/2}$, and 3.5×10^{5} cm Hz$^{1/2}$/W, respectively. The enhanced photocurrent response under illumination at the blue–green wavelength is primarily attributed to the photoexcitation of E'_δ defects in BSO:Si$^+$. The EPR analysis proves the existence and evolution of E'_δ defect, which strongly supports the observed enhancement in photoconductivity of the BSO:Si$^+$. The etching-depth-dependent photocurrent supports the TRIM calculated depth-distribution profile of excess Si atoms in BSO:Si$^+$.

This work was supported by the National Science Council (NSC) of the Republic of China under Grant No. NSC92-2215-E-009-028.

[1]H. Z. Song, X. M. Bao, N. S. Li, and J. Y. Zhang, J. Appl. Phys. **82**, 4028 (1997).
[2]H. S. Bae, T. G. Kim, C. N. Whang, S. Im, J. S. Yun, and J. H. Song, J. Appl. Phys. **91**, 4078 (2002).
[3]S. Cheylan and R. G. Elliman, Appl. Phys. Lett. **78**, 1225 (2001).
[4]H. Nishikawa, R. Nakamura, and J. H. Stathis, Phys. Rev. B **60**, 15910 (1999).
[5]H. Z. Song and X. M. Bao, Phys. Rev. B **55**, 6988 (1997).
[6]G.-R. Lin, Jpn. J. Appl. Phys., Part 2 **41**, L1379 (2002).
[7]G.-R. Lin, J. Appl. Phys. **94**, 7542, (2003).
[8]S. H. Choi and R. G. Elliman, Appl. Phys. Lett. **74**, 3987 (1999).
[9]Y. Hirano, F. Sato, S. Aihara, N. Saito, S. Miyazaki, and M. Hirose, Appl. Phys. Lett. **79**, 2255 (2001).
[10]S. Coffa, A. Polman, and O. Soref, Mater. Res. Soc. Symp. Proc. **486**, 337 (1998).
[11]G. Pacchioni and G. Ierano, Phys. Rev. Lett. **81**, 377 (1998).
[12]H. Nishikawa, E. Watanabe, D. Ito, Y. Sakurai, K. Nagasawa, and Y. Ohki, J. Appl. Phys. **80**, 3513 (1996).
[13]M. Y. Valakh, V. A. Yukhimchuk, V. Y. Bratus, A. A. Konchits, P. L. F. Hemment, and T. Komoda, J. Appl. Phys. **85**, 168 (1999).
[14]L. Skuja, J. Non-Cryst. Solids **239**, 16 (1998).

This article is copyrighted as indicated in the article. Reuse of AIP content is subject to the terms at: http://scitation.aip.org/termsconditions. Downloaded to IP: 140.113.38.11 On: Thu, 01 May 2014 04:15:37